Rationalizing the alkali ions distribution along the honeycomb layered (Li,Na)2SnO3 pseudo solid solution

Romain Berthelot, Carla Crobu, Eunice Mumba Mpanga, Bernard Fraisse, Marie-Liesse Doublet

Rationalizing the alkali ions distribution along the honeycomb layered $(Li,Na)_2SnO_3$ pseudo solid solution

Romain Berthelot,[1,2]* Carla Crobu,[1] Eunice Mumba Mpanga,[1,2] Bernard Fraisse,[1,2] Marie-Liesse Doublet[1,2]

1 : ICGM, Univ Montpellier, CNRS, ENSCM, Montpellier, France

2 : Réseau sur le Stockage Électrochimique de l'Énergie (RS2E), CNRS, Amiens, France

Corresponding author:

Dr. Romain Berthelot: romain.berthelot@umontpellier.fr

Abstract

Alkali-rich layered oxides Li_2SnO_3 and Na_2SnO_3 are isostructural, but no alkali-mixed compositions have been reported so far. While the thermodynamic stability of such mixed compositions is predicted by DFT calculations mainly for the sodium-rich side, single-phase compounds $Li_{2-x}Na_xSnO_3$ were successfully obtained in the whole composition range ($0 \leq x \leq 2$) by conventional solid-state synthesis thanks to a quenching procedure at the end of the heat treatment. From Li_2SnO_3 to Na_2SnO_2, the evolution of the cell parameters and the DFT calculations demonstrate that the lithium-to-sodium substitution occurs firstly inside the alkali layer up to $Li_{0.5}Na_{1.5}SnO_3$ and then in the honeycomb layer.

Keywords

alkali transition metal layered oxide, honeycomb ordering, density functional theory calculations, solid solution

Introduction

Alkali-rich and honeycomb-ordered layered oxides with the general chemical formula A_2MO_3 (with A being an alkali metal and M a (post)transition metal) are part of the vast family of layered compounds, widely investigated especially as battery electrode materials.[1,2] Their crystal structure is usually described as an alternate stacking of edge-shared octahedra layers in the so-called O3-type stacking.[3] The (post)transition metal layers exhibit an in-plane honeycomb-like cationic ordering with each AO_6 octahedron surrounded by six MO_6 octahedra, whereas the alkali layers only consists of AO_6 octahedra. Due to the honeycomb ordering, various stacking sequences are possible, leading in some cases to stacking faults which may alter the diffraction patterns and modify the electrochemical behavior, as it has been extensively investigated for the electrode material Li_2MnO_3.[4–8]

Remarkably, there are only few examples of alkali-mixed transition metal layered oxides. In early 2000s, single crystals of titanates containing both lithium and sodium cations have been grown by Nalbandyan and coworkers.[9] Matsumura *et al.* and later Holzapfel *et al.* also reported some alkali-mixed compositions in the same system.[10,11] Focusing now on honeycomb-ordered layered systems, some of us evidenced a complete solid-solution between the analogs $LiNi_{2/3}Sb_{1/3}O_2$ and $NaNi_{2/3}Sb_{1/3}O_2$ with a random distribution of lithium and sodium cations inside the alkali layer. Importantly, these alkali-mixed compositions are shown to be metastable with respect to phase segregation. Indeed, a quenching at the end of the high-temperature solid-state synthesis is necessary to avoid phase segregation and enable to get a single-phase end product.[12] Recently, the group of Tarascon reported the thermodynamically stable alkali-mixed compositions $Li_{0.5}Na_{1.5}IrO_3$ and $Li_{0.5}Na_{1.5}MnO_3$, with lithium and sodium ions lying exclusively in the transition metal layer and in the alkali layer, respectively.[13,14] Note that similar results were obtained by the same group with the unique layered sulfide analog $Li_{0.5}Na_{1.5}TiS_3$[15].

From a fundamental point of view, understanding the thermodynamic factors stabilizing alkali-mixed layered compositions is critical as these materials might exhibit enhanced electrochemical properties compared to their pure lithium or sodium analogs. Among these factors, the size of the alkali ions is the most obvious and explains the preference of lithium rather than sodium to preferentially lie in the metallic honeycomb layer.

In this context, we explore the model system $Li_2SnO_3 – Na_2SnO_3$, with tin in being electrochemically inactive, to check the possible promotion of other alkali cation distributions with post-transitional elements. To the best of our knowledge, no alkali-mixed $Li_{2-x}Na_xSnO_3$ compositions have been reported so far, in spite of Li_2SnO_3 and Na_2SnO_3 being isostructural. Herein, we compute and rationalize the $Li_2SnO_3 – Na_2SnO_3$ phase diagram through density functional theory calculations and determine the thermodynamic (meta)stability domains of this system. Accordingly, conventional solid-state methods with final quenching at the end of the heat treatment were used to reach single-phase compositions in the whole composition range from Li_2SnO_3 to Na_2SnO_3. Instead of a classical solid-solution behavior, a non-linear evolution of the cell parameters is experimentally observed that is explained by different configurations of alkali ions distribution according to the chemical composition (more precisely the respective content of alkali ions).

Computational and experimental details

Density functional theory (DFT) calculations were performed using the VASP program package [17] using PAW pseudopotentials[18] for the atom description and the PBE generalized gradient approximation[19] for the exchange and correlation potential. The crystallographic structure of Li_2SnO_3 provided by Hoppe and coworkers[20] was considered as the starting model (monoclinic space group *C*2/*c*, Figure 1) from which the $Li_{2-x}Na_xSnO_3$ composition was varied

in the range $0 \leq x \leq 2$ through a progressive lithium for sodium substitution. For each composition, different distributions of lithium and sodium cations were generated depending on the substituted alkali sites 4*e* (within the two honeycomb layers), 4*d* and 8*f* (within the two alkali layers) (Figure 1c). All structural relaxations were performed on a supercell containing 12 formula units using the conjugate gradient method with a convergence criteria of 2.10^{-3} eV/Å^{-1} for the atomic forces. The plane-waves energy cutoff was set to 600 eV and a k-point grid density of at least 1000/at

Solid-state syntheses were performed by heating powder mixtures of pre-dried alkali carbonates (Li_2CO_3, Alfa Aesar 99% and Na_2CO_3, Alfa Aesar 98%) and tin oxide (SnO_2, Merck 99.9%). The mixture was homogenized by mechanical milling (20 minutes in a SPEX 8000) and then pelletized before the heat treatment at 800 C in air in muffle furnace. A nominal 15 % excess of carbonates was necessary to balance the alkali volatility and to avoid remaining traces of SnO_2 after the synthesis.

X-ray powder diffraction (XRPD) patterns were collected on PANalytical Empyrean diffractometer with cupper radiation. The thermal behavior of particular compositions was also followed by *in situ* XRPD with an Anton Paar heating chamber. To do so, powder suspensions were deposited and then evaporated onto platinum blade, the latter being heated up to 800 C with dwell every 100 °C for XRPD acquisition.

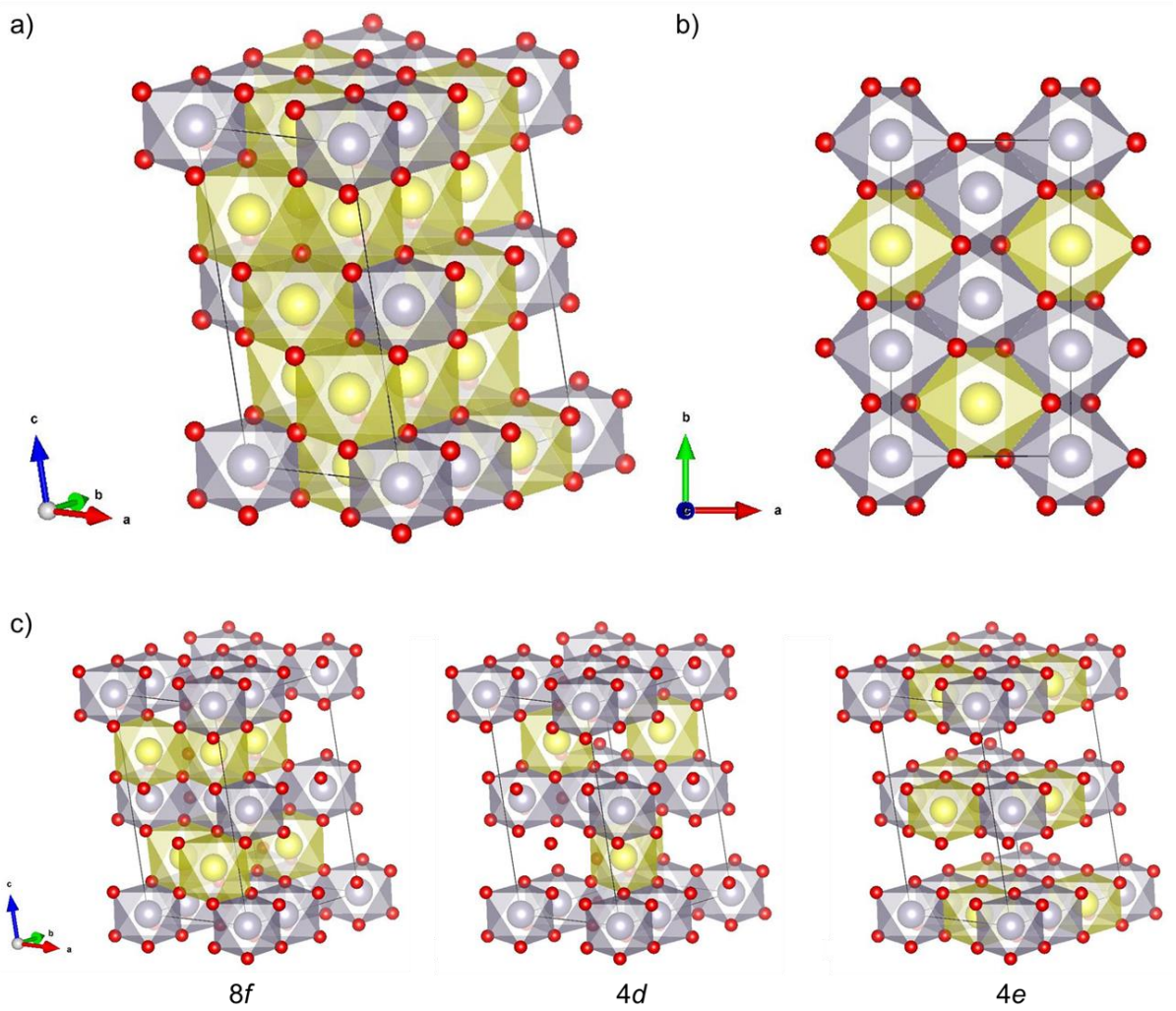

Figure 1: Crystal structure of Li_2SnO_3 adapted from Ref.[20] (a) with its top-view to highlight the particular Sn/Li cationic ordering (b) and the three crystallographic sites for lithium cations (c).

Results

Figure 2 shows the formation energy of the relaxed $Li_{2-x}Na_xSnO_3$ configurations ($0 \leq x \leq 2$) with respect to the proportional mixture of Li_2SnO_3 ($x = 0$) and Na_2SnO_3 ($x = 2$). For a sake of clarity, the structures with n sodium atoms in the honeycomb layers ($n = 0$ to 4 in the 4*e* Wyckoff sites) are highlighted with different colors. Starting from Li_2SnO_3, the progressive substitution of lithium for larger sodium cations invariably leads to an energy destabilization. As expected from the larger ionic radius of Na^+ compared to Sn^{4+} (1.02 Å *vs.* 0.69 Å)[16], the

destabilization increases with the number of sodium cations in the honeycomb layer (for example, see Figure S1 for the particular composition $Li_{1.5}Na_{0.5}SnO_3$) up to the critical composition $Li_{0.5}Na_{1.5}SnO_3$ above which no more structures with $n = 0$ can be generated. The most stable composition is found when lithium and sodium cations are fully ordered in the honeycomb and the alkali layers, respectively (*i.e.* lithium in 4*e* site, sodium in 4*f* and 8*d* sites), exactly like the thermodynamically stable analogs $NaLi_{1/3}Ir_{2/3}O_2$ [10] and $NaLi_{1/3}Mn_{2/3}O_2$.[11]

Interestingly, thermodynamically (meta)stable phases are found for $x < 1.5$, when no sodium cations are introduced in the honeycomb layer (blue circles in Figure 2). Among them, those having a negative or slightly positive formation energies falling in the room temperature thermal energy (25 meV) show a partial ordering of the sodium cations in one of the two alkali layers rather than a homogeneous distribution over the two alkali layers. This ordering shows that the system energy is less penalized when the strain induced by the sodium ions concerns only one of the two alkali layers.

Moving to sodium-rich compositions, from $Li_{0.5}Na_{1.5}SnO_3$ to Na_2SnO_3, a solid-solution is predicted with sodium cations progressively entering the remaining 4*e* sites of the honeycomb layer.

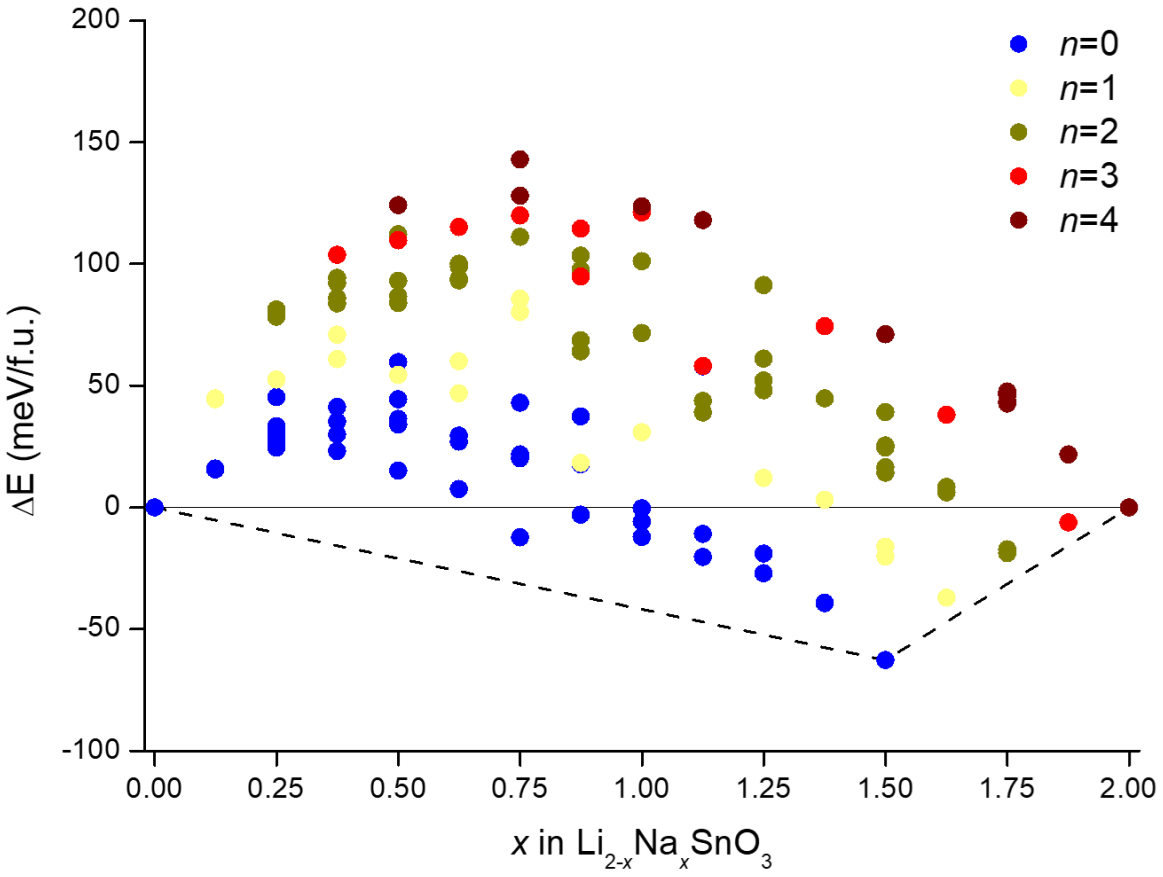

Figure 2: Formation energy (meV/f.u.) of the $Li_{2-x}Na_xSnO_3$ single-phases with respect to the stoichiometric mixture of Li_2SnO_3 and Na_2SnO_3, as obtained from DFT calculations. For each composition, various distributions of alkali cations within the honeycomb and/or alkali layers were considered and are here classified as a function of the number of sodium cations lying in the honeycomb layer (n ranging from 0 to 4, irrespectively of the distribution in the two different honeycomb layers).

Previous experimental works clearly revealed that a final quenching at the end of the solid-state synthesis enable to stabilize metastable alkali-mixed layered compositions at room temperature. This is the case for example for the compositions $Li_{1-x}Na_xNi_{2/3}Sb_{1/3}O_2$ ($0 \leq x \leq 1$) and for the alkali-ordered $Li_xNa_yCoO_2$, which both tend to decompose in a Li-rich and a Na-rich phases when submitted to a slow cooling process.[12,21] In that context, and according to the computational investigation described above, solid-state syntheses of $Li_{2-x}Na_xSnO_3$ (x = 0, 0.5, 1, 1.5 and 2) target compositions were ended by quickly removing the pellet out of the furnace and a subsequently grinding at room temperature in an agate mortar. Figure 3 gathers the

corresponding XRPD patterns. The synthesis of both Li_2SnO_3 and Na_2SnO_3 is confirmed, with no trace of impurities or remaining precursors and with refined cell parameters in agreement with the literature, although significant amount of stacking faults altering the pattern of Na_2SnO_3 hence preventing from an accurate profile matching refinement. It is then interesting to look at the XRPD patterns of the three intermediate compositions $Li_{1.5}Na_{0.5}SnO_3$, $LiNaSnO_3$ and $Li_{0.5}Na_{1.5}SnO_3$. All of them could be also well indexed with the same monoclinic space group *C* 2/*c*. The presence of a unique (002) intense peak around 17 ° clearly demonstrates that the three compositions are single-phase. Finally, at low angles no additional superstructure peak could be detected. The hypothesis of an alternation of distinct alkali layers, as observed in $Li_xNa_yCoO_2$,[21] or more recently in the P2-type phase $NaKNi_2TeO_6$,[22,23] could be reasonably discarded.

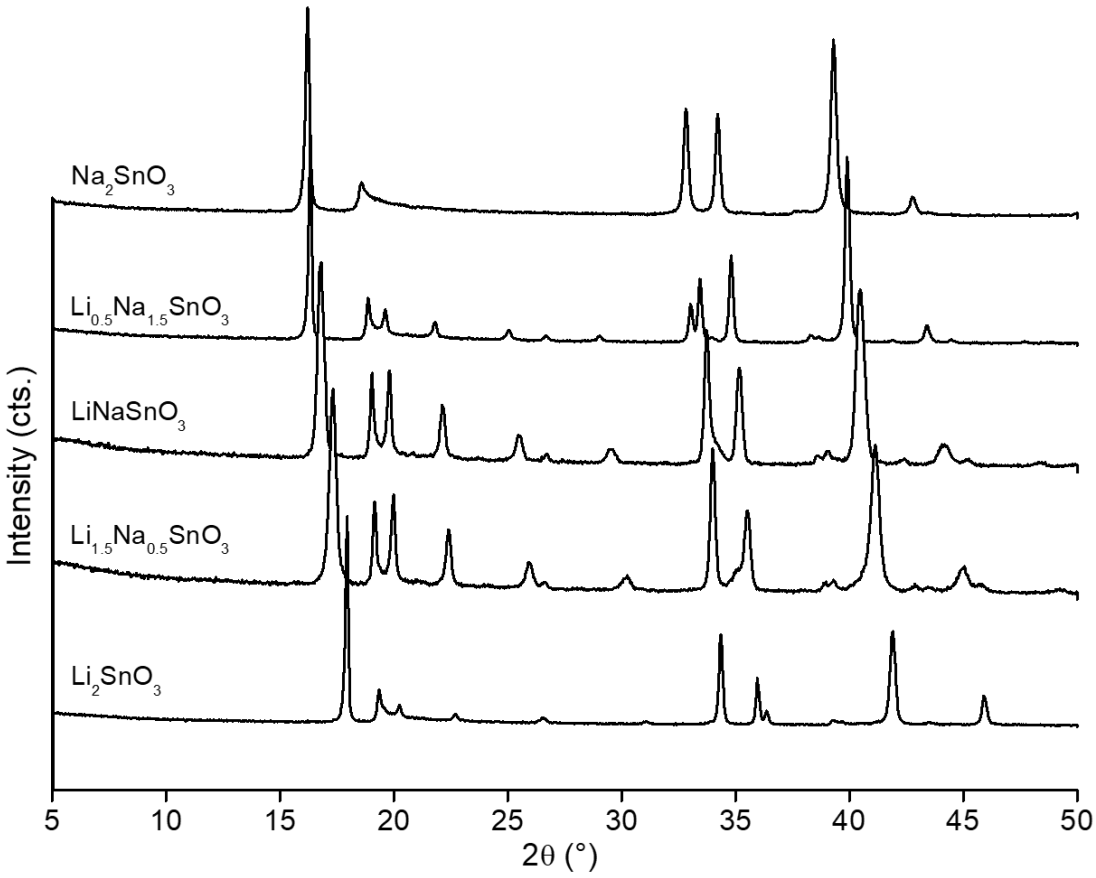

Figure 3: XRPD patterns on 5 – 50 ° 2θ range collected for different compositions from Li_2SnO_3 (bottom) to Na_2SnO_3 (top).

Discussion

The above results confirm that it is possible to obtain single-phase alkali-mixed compounds $Li_{2-x}Na_xSnO_3$ in the whole composition range, even though the phase stability diagram obtained from T = 0K DFT calculations predicts only Na-rich single phases to be stable towards phase segregation. It is now interesting to figure out how the alkali substitution proceeds from Li_2SnO_3 to Na_2SnO_3. The computational investigation of $Li_{2-x}Na_xSnO_3$ formation energies shows less destabilized configurations when no sodium cations occur in the honeycomb layer, up to the critical composition $Li_{0.5}Na_{1.5}SnO_3$. However, configurations with $n > 0$ cannot be fully excluded when their formation energy falls in the room temperature thermal energy. We then focused on the structural parameters obtained after structural relaxation to check the possible ordering of the alkali ions in the structure. It is well known that the nature and the amount of the alkali element strongly influence the hexagonal *c*-axis parameter in alkali transition metal layered compounds. While the thickness of the transition metal layer does not evolve significantly from one element to another because of very close ionic radii, the alkali interlayer thickness can be extended from a layer of lithium ions in octahedral symmetry to a layer of potassium ions in prismatic sites. In honeycomb-ordered layered compounds often described in a monoclinic cell, it is then interesting to pay attention to the parameter $c \cdot \sin(\beta)$ to estimate the thickness of the layers. The evolution of this last parameter is gathered Figure S2 for the most stable configurations obtained after structural relaxation with *n* ranging from 0 to 4. For each *n* a linear trend is observed, which is indicative of a classic solid-solution behavior following a Vegard law. Noteworthy, for any given Na/Li substitution content, the $c.\sin(\beta)$ parameter decreases with *n*, while the phase formation energy increases (Figure 2). This suggests that the thickness of the metallic layers is less sensitive to Na/Li substitution than the alkali layer or equivalently that the expansion of the c-lattice parameter of mixed layered

structures is primarily governed by the alkali layers. Combining the energetical and structural analysis, it is then expected that the Na/Li substitution in $Li_{2-x}Na_xSnO_3$ structures preferentially occurs within the alkali layers up to the critical $Li_{0.5}Na_{1.5}SnO_3$ composition, resulting in a Vegard-type expansion of the c-lattice parameter. Above this composition, the remaining Na/Li substitution takes place in the metallic layers which causes a deviation from the Vegard law.

We then scrutinized the evolution of the cell parameters obtained from XRPD profile matching refinement. Multiple series of synthesis have been performed, with also additional Li/Na proportions in order to increase the statistics (Figures 4 and S3). The evolution of the monoclinic cell volume follows a clear linear trend, which could be linked to a classic solid-solution behavior by the lithium to sodium substitution, irrespectively of the substitution ratio. However, the $c\cdot\sin(\beta)$ parameter clearly show two linear domains below and above the critical $Li_{0.5}Na_{1.5}SnO_3$ composition. The one-to-one mapping of the experimental and theoretical results is not relevant as DFT calculations are performed at T = 0K. Nevertheless, the structural trends deduced from the DFT investigation is fully consistent with the evolution of the experimental cell parameters regarding the distribution of lithium and sodium ions in the structure. The important increase of $c\cdot\sin(\beta)$ from Li_2SnO_3 to $Li_{0.5}Na_{1.5}SnO_3$ shown in Figure 4 is induced by a random lithium to sodium substitution in the alkali layers, consistent with the significant broadening of the (0 0 2) peak observed in the XRPD pattern of Figure 3. Further substitutions for Na-richer compositions inevitably occur inside the honeycomb layers, with a very limited increase of the parameter $c\cdot\sin(\beta)$. The fact that the deviation from the Vegard law is observed in the $c\cdot\sin(\beta)$ parameter and not in the cell volume is due to a compensation of the a- and b-lattice parameters compared to $c\cdot\sin(\beta)$. While the two former also deviate from the Vegard law above the critical $Li_{0.5}Na_{1.5}SnO_3$ composition, they increase to accommodate the Na ions.

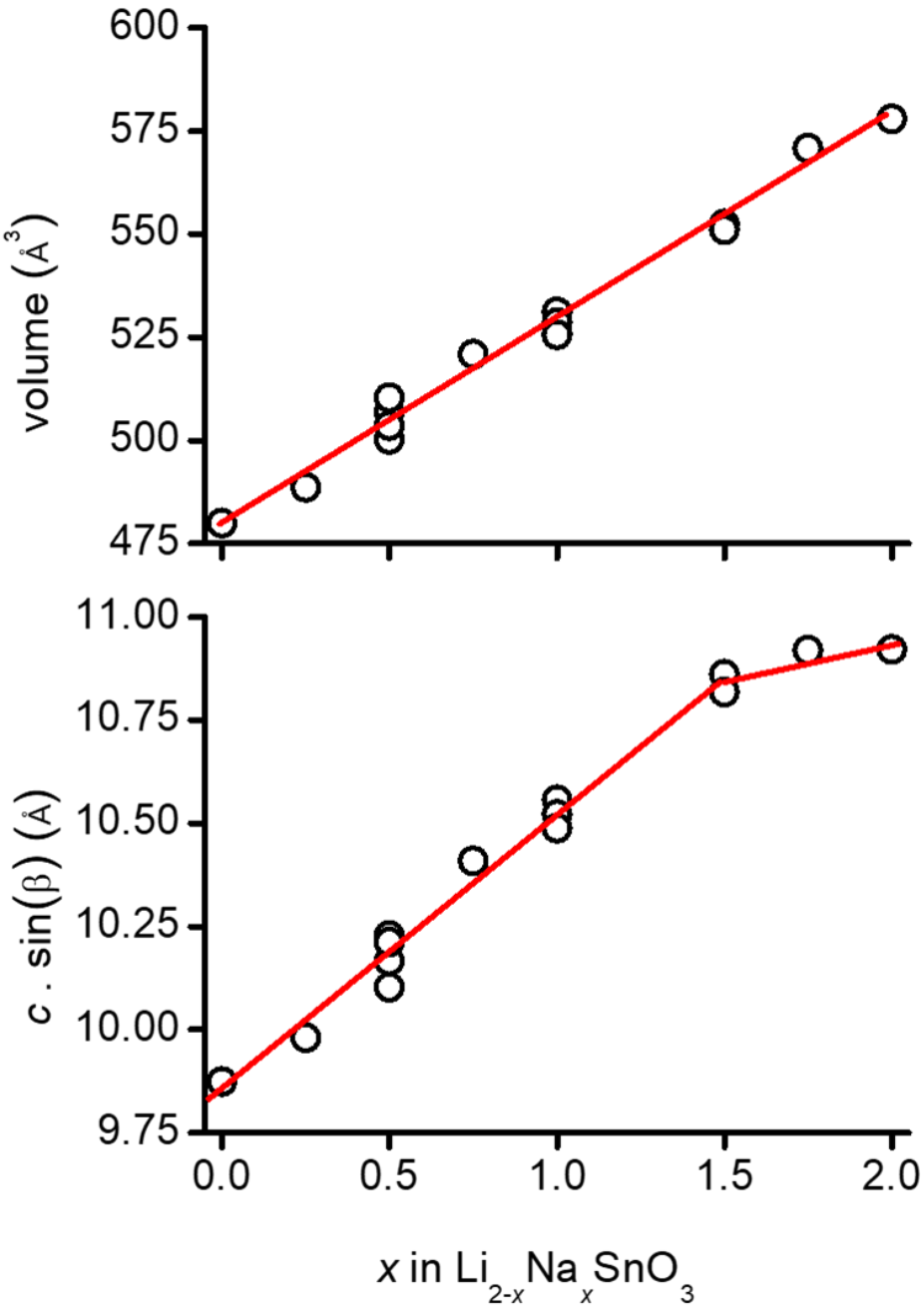

Figure 4: Evolution of the volume of the monoclinic cell and the parameter $c \cdot \sin(\beta)$ with increasing amount of sodium from XRPD profile matching refinement collected for various series of solid-state syntheses.

The last section of our investigation deals with the thermal stability of the peculiar alkali-mixed compositions $LiNaSnO_3$ and $Li_{0.5}Na_{1.5}SnO_3$. According to our DFT phase stability diagram both phases are thermodynamically stable with respect to the phase segregation into Li_2SnO_3 and Na_2SnO_3. However, the former is metastable towards its decomposition into Li_2SnO_3 and

$Li_{0.5}Na_{1.5}SnO_3$, as its energy is +22 meV/f.u. above the reference energy of this biphasic domain (see the dotted line in Figure 2). The thermal evolution of these alkali-mixed compositions was then checked by *in situ* XRD (Figure 5). At 300 °C the diffraction peak (0 0 2) of $LiNaSnO_3$ splits into two distinct contributions. Around 600 °C, the two contributions merge into a unique peak. During the slow cooling process, this unique peak decomposes again into two contributions, with final 2θ positions around 16.6° and 18.0° at room temperature which correspond to the (0 0 2) peaks of $Li_{0.5}Na_{1.5}SnO_3$ and Li_2SnO_3, respectively. When the same procedure is applied to the $Li_{0.5}Na_{1.5}SnO_3$, no peak splitting is observed upon heating, but a small shift of the (0 0 2) peak to lower angles due to the thermal expansion. This second composition is therefore dynamically stable upon phase segregation into a Li-rich and a Na-rich phases, as for its iridium and manganese analogs.[14,24] These results confirm the accuracy and reliability of our DFT phase stability diagram.

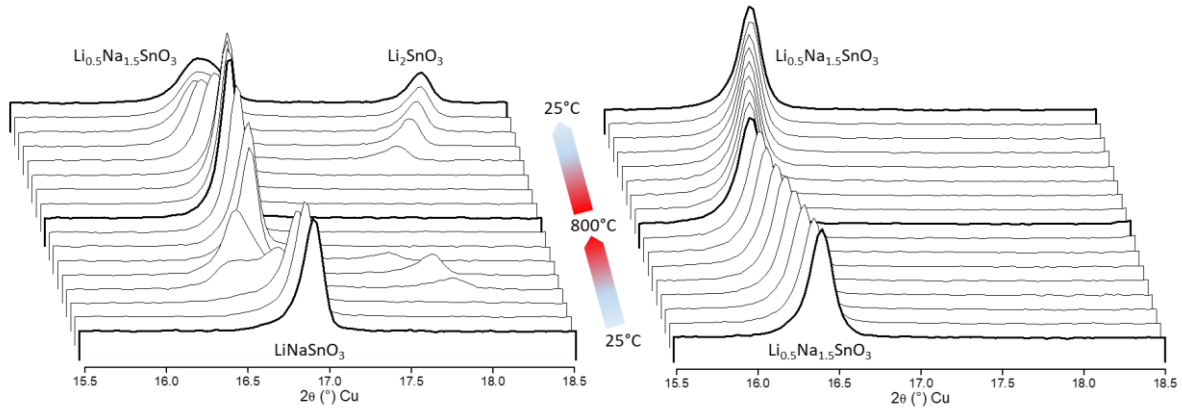

Figure 5: Evolution of the XRD patterns of $LiNaSnO_3$ (left) and $Li_{0.5}Na_{1.5}SnO_3$ as a function of the temperature (with a step of 100 ° between each pattern).

Conclusion

In the search for new alkali-mixed layered compositions, a complete solid solution between Li_2SnO_3 and Na_2SnO_3 could be prepared by classic solid-state reactions. The final quenching

at the end of the heat treatment enables to stabilize metastable compositions which were found higher in energy than the convex hull of the Li-Na-Sn-O phase stability diagram obtained from DFT calculations. The difference in the ionic radii of Li^+ and Na^+, but also Na^+ and Sn^{4+}, drives the lithium to sodium substitution between the available sites of the alkali or honeycomb layers with sodium preferentially filling the former. The mechanical strain of the honeycomb layer due to the Na for Li substitution is shown to be too penalizing to stabilize fully disordered phases with sodium ions lying both in the metallic and alkali layers. Instead, a solid solution between the Li_2SnO_3 and the $Li_{0.5}Na_{1.5}SnO_3$ end-members is obtained thanks to a final temperature quenching. This result confirms the richness of alkali-mixed layered compositions and should encourage the investigation of other layered systems AMO_2 with A being lithium, sodium and potassium. On the specific alkali-rich tin-based compounds, the investigation should be transferred to the sulfide system Li_2SnS_3-Na_2SnS_3 for which interesting ionic conductivities have been reported recently.[25–27]

Acknowledgements

The authors thank the French National Research Agency (STORE-EX Labex Project ANR-10-LABX-76-01) for financial support and for the development of the Q-cats platform for DFT calculation. RB wants to acknowledge Majda Gribi for the preliminary experimental work.

References

(1) Abakumov, A. M.; Fedotov, S. S.; Antipov, E. V; Tarascon, J.-M. Solid State Chemistry for Developing Better Metal-Ion Batteries. *Nat. Commun.* **2020**, *11* (1), 4976. https://doi.org/10.1038/s41467-020-18736-7.

(2) Zhang, H.; Li, C.; Eshetu, G. G.; Laruelle, S.; Grugeon, S.; Zaghib, K.; Julien, C.; Mauger, A.; Guyomard, D.; Rojo, T.; et al. From Solid-Solution Electrodes and the Rocking-Chair Concept to

Today's Batteries. *Angew. Chemie Int. Ed.* **2020**, *59* (2), 534–538. https://doi.org/https://doi.org/10.1002/anie.201913923.

(3) Delmas, C.; Fouassier, C.; Hagenmuller, P. Structural Classification and Properties of the Layered Oxides. *Phys. B+C* **1980**, *99* (1–4), 81–85. https://doi.org/10.1016/0378-4363(80)90214-4.

(4) Bréger, J.; Jiang, M.; Dupré, N.; Meng, Y. S.; Shao-Horn, Y.; Ceder, G.; Grey, C. P. High-Resolution X-Ray Diffraction, DIFFaX, NMR and First Principles Study of Disorder in the Li2MnO3-Li[Ni1/2Mn1/2]O2 Solid Solution. *J. Solid State Chem.* **2005**, *178* (9), 2575–2585.

(5) Boulineau, A.; Croguennec, L.; Delmas, C.; Weill, F. Reinvestigation of Li2MnO3 Structure: Electron Diffraction and High Resolution TEM. *Chem. Mater.* **2009**, *21* (18), 4216–4222. https://doi.org/10.1021/cm900998n.

(6) Boulineau, A.; Croguennec, L.; Delmas, C.; Weill, F. Structure of Li2MnO3 with Different Degrees of Defects. *Solid State Ionics* **2010**, *180* (40), 1652–1659. https://doi.org/10.1016/j.ssi.2009.10.020.

(7) Matsunaga, T.; Komatsu, H.; Shimoda, K.; Minato, T.; Yonemura, M.; Kamiyama, T.; Kobayashi, S.; Kato, T.; Hirayama, T.; Ikuhara, Y.; et al. Dependence of Structural Defects in Li2MnO3 on Synthesis Temperature. *Chem. Mater.* **2016**, *28* (12), 4143–4150. https://doi.org/10.1021/acs.chemmater.5b05041.

(8) Serrano-Sevillano, J.; Carlier, D.; Saracibar, A.; Lopez del Amo, J. M.; Casas-Cabanas, M. DFT-Assisted Solid-State NMR Characterization of Defects in Li2MnO3. *Inorg. Chem.* **2019**, *58* (13), 8347–8356. https://doi.org/10.1021/acs.inorgchem.9b00394.

(9) Shilov, G. V.; Nalbandyan, V. B.; Volochaev, V. A.; Atovmyan, L. O. Crystal Growth and Crystal Structures of the Layered Ionic Conductors-Sodium Lithium Titanium Oxides. *Int. J. Inorg. Mater.* **2000**, *2* (5), 443–449. https://doi.org/10.1016/S1466-6049(00)00050-7.

(10) Matsumura, T.; Kanno, R.; Gover, R.; Kawamoto, Y.; Kamiyama, T.; Mitchell, B. J. Synthesis, Structure and Physical Properties of $Li_xNa_{1-x}NiO_2$. *Solid State Ionics* **2002**, *152–153*, 303–309.

(11) Holzapfel, M.; Darie, C.; Bordet, P.; Chappel, E.; Núñez-Regueiro, M. D.; Diaz, S.; De Brion, S.; Chouteau, G.; Strobel, P. Mixed Layered Oxide Phases Na XLi 1-XNiO 2: A Detailed Description of Their Preparation and Structural and Magnetic Identification. *Solid State Sci.* **2005**, *7* (5), 497–506. https://doi.org/10.1016/j.solidstatesciences.2004.10.046.

(12) Vallée, C.; Saubanère, M.; Sanz-Camacho, P.; Biecher, Y.; Fraisse, B.; Suard, E.; Rousse, G.; Carlier, D.; Berthelot, R. Alkali-Glass Behavior in Honeycomb-Type Layered Li<inf>3-X</Inf>Na<inf>x</Inf>Ni<inf>2</Inf>SbO<inf>6</Inf> Solid Solution. *Inorg. Chem.* **2019**, *58* (17). https://doi.org/10.1021/acs.inorgchem.9b01385.

(13) Perez, A. J.; Rousse, G.; Tarascon, J.-M. Structural Instability Driven by Li/Na Competition in Na(Li1/3Ir2/3)O2 Cathode Material for Li-Ion and Na-Ion Batteries. *Inorg. Chem.* **2019**, *58* (22), 15644–15651. https://doi.org/10.1021/acs.inorgchem.9b02722.

(14) Wang, Q.; Mariyappan, S.; Rousse, G.; Morozov, A. V; Porcheron, B.; Dedryvère, R.; Wu, J.; Yang, W.; Zhang, L.; Chakir, M.; et al. Unlocking Anionic Redox Activity in O3-Type Sodium 3d Layered Oxides via Li Substitution. *Nat. Mater.* **2021**, *20* (3), 353–361. https://doi.org/10.1038/s41563-020-00870-8.

(15) Leube, B. T.; Salager, E.; Chesneau, E.; Vezin, H.; Abakumov, A. M.; Tarascon, J. Layered Sodium Titanium Trichalcogenide Na 2 TiCh 3 Framework (Ch = S, Se): A Rich Crystal and Electrochemical Chemistry. *Chem. Mater.* **2022**, *34*, 2382–2392.

(16) Shannon, R. D. Revised Effective Ionic Radii and Systematic Studies of Interatomic Distances in Halides and Chalcogenides. *Acta Crystallogr. Sect. A Found. Crystallogr.* **1976**, *32* (5), 751–767. https://doi.org/10.1107/S0567739476001551.

(17) Kresse, G.; Furthmuller, J. Efficiency of Ab-Initio Total Energy Calculations for Metals and Semiconductors Using a Plane-Wave Basis Set. *Comput. Mater. Sci.* **1996**, *6* (1), 15–50.

(18) G.Kresse, D. J. From Ultrasoft Pseudopotentials to the Projector Augmented-Wave Method. *Phys. Rev. B* **1999**, *59* (3), 1758–1775. https://doi.org/10.1103/PhysRevB.59.1758.

(19) Perdew, J. P.; Burke, K.; Ernzerhof, M. Generalized Gradient Approximation Made Simple. *Phys. Rev. Lett.* **1996**, *77* (18), 3865–3868. https://doi.org/10.1103/PhysRevLett.77.3865.

(20) Kreuzburg, G.; Stewner, F.; Hoppe, R. Die Kristallstruktur von Li2SnO3. *Z. anorg. allg. Chem.* **1971**, *379* (3), 242–254.

(21) Berthelot, R.; Pollet, M.; Carlier, D.; Delmas, C. Reinvestigation of the OP4-(Li/Na)CoO2-Layered System and First Evidence of the (Li/Na/Na)CoO2 Phase with OPP9 Oxygen Stacking. *Inorg. Chem.* **2011**, *50* (6), 2420–2430. https://doi.org/10.1021/ic102218w.

(22) Masese, T.; Miyazaki, Y.; Rizell, J.; Kanyolo, G. M.; Chen, C.-Y.; Ubukata, H.; Kubota, K.; Sau, K.; Ikeshoji, T.; Huang, Z.-D.; et al. Mixed Alkali-Ion Transport and Storage in Atomic-Disordered Honeycomb Layered NaKNi2TeO6. *Nat. Commun.* **2021**, *12* (1), 4660. https://doi.org/10.1038/s41467-021-24694-5.

(23) Berthelot, R.; Serrano-Sevillano, J.; Fraisse, B.; Fauth, F.; Weill, F.; Laurencin, D.; Casas-Cabanas, M.; Carlier, D.; Rousse, G.; Doublet, M.-L. Stacking Versatility in Alkali-Mixed Honeycomb Layered NaKNi2TeO6. *Inorg. Chem.* **2021**, *60* (18), 14310–14317. https://doi.org/10.1021/acs.inorgchem.1c01876.

(24) Perez, A. J.; Rousse, G.; Tarascon, J. M. Structural Instability Driven by Li/Na Competition in Na(Li1/3Ir2/3)O2 Cathode Material for Li-Ion and Na-Ion Batteries. *Inorg. Chem.* **2019**. https://doi.org/10.1021/acs.inorgchem.9b02722.

(25) Kuhn, A.; Holzmann, T.; Nuss, J.; Lotsch, B. V. A Facile Wet Chemistry Approach towards Unilamellar Tin Sulfide Nanosheets from Li4xSn1−xS2 Solid Solutions. *J. Mater. Chem. A* **2014**, *2* (17), 6100–6106. https://doi.org/10.1039/C3TA14190J.

(26) Brant, J. A.; Massi, D. M.; Holzwarth, N. A. W.; Macneil, J. H.; Douvalis, A. P.; Bakas, T.; Martin, S. W.; Gross, M. D.; Aitken, J. A. Fast Lithium Ion Conduction in Li2SnS3: Synthesis, Physicochemical Characterization, and Electronic Structure. *Chem. Mater.* **2015**, *27* (1), 189–196. https://doi.org/10.1021/cm5037524.

(27) Holzmann, T.; Schoop, L. M.; Ali, M. N.; Moudrakovski, I.; Gregori, G.; Maier, J.; Cava, R. J.; Lotsch, B. V. Li0.6[Li0.2Sn0.8S2]-a Layered Lithium Superionic Conductor. *Energy Environ. Sci.* **2016**, *9* (8), 2578–2585. https://doi.org/10.1039/c6ee00633g.